ACS Chemical Neuroscience

pubs.acs.org/chemneuro Research Article

In Vitro Evaluation of [^{3}H]CPPC as a Tool Radioligand for CSF-1R

Ashley C. Knight, Cassis Varlow, Tong Zi, Steven H. Liang, Lee Josephson, Karl Schmidt, Shil Patel,* and Neil Vasdev*

Cite This: https://dx.doi.org/10.1021/acschemneuro.0c00802 Read Online

ACCESS | Metrics & More | Article Recommendations | Supporting Information

ABSTRACT: Microglia play a role in several central nervous system (CNS) diseases and are a highly sought target for positron emission tomography (PET) imaging and therapeutic intervention. 5-Cyano-*N*-(4-(4-[^{11}C]methylpiperazin-1-yl)-2-(piperidin-1-yl)phenyl)furan-2-carboxamide ([^{11}C]CPPC) is a radiopharmaceutical designed to selectively target microglia *via* macrophage colony stimulating factor-1 receptor (CSF-1R) in the CNS. Herein, we report the first preclinical evaluation of [^{3}H]CPPC using radioligand binding methods for the evaluation of putative CSF-1R inhibitors in rodent models of neuroinflammation. The distribution of [^{3}H]CPPC by autoradiography did not align with 18 kDa translocator protein (TSPO) distribution using [^{3}H]PBR28 and IBA-1 staining for microglia. In the CNS, [^{3}H]CPPC had considerable nonspecific binding, as indicated by a low displacement of the tritiated ligand by unlabeled CPPC and the known CSF1R inhibitors BLZ-945 and PLX3397. Spleen was identified as a tissue that provided an adequate signal-to-noise ratio to enable screening with [^{3}H]CPPC and a library of 20 novel PLX3397 derivatives. However, unlabeled CPPC lacked selectivity and showed off-target binding to a substantial number of kinase targets (204 out of 403 tested) at a concentration relevant to *in vitro* radioligand binding assays (10 μM). These findings suggest that, while [^{3}H]CPPC may have utility as a radioligand tool for the evaluation of peripheral targets and screening of CSF-1R inhibitors, it may have limited utility as an *in vivo* CNS imaging probe on the basis of the current evaluation.

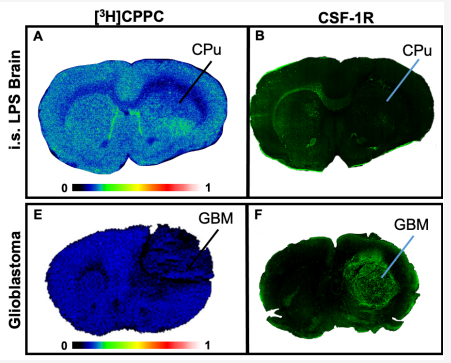

KEYWORDS: *Positron emission tomography, PET, CSF-1R, autoradiography, CPPC, colony stimulating factor-1 receptor, in vitro*

INTRODUCTION

Macrophage colony stimulating factor-1 receptor (CSF-1R), also referred to as CD-115, is a receptor tyrosine kinase localized to the extracellular membrane of microglia, a small number of neurons, and peripheral macrophages.[1−3] In the brain, CSF-1R signaling is mediated by two endogenous ligands, colony stimulating factor-1 (CSF-1) and interleukin-34 (IL-34), contributing to microglial migration, survival, and proliferation.[3,4] CSF-1R signaling is hypothesized to activate and enlist macrophages to a site of injury,[5] making CSF-1R an important therapeutic target. In Alzheimer's disease (AD), CSF-1R expression is increased,[6,7] and studies have shown beneficial effects of CSF-1R inhibition on neurodegeneration and neuroinflammation.[8−12] Multiple efforts are ongoing to explore CSF-1R inhibitors in the central nervous system (CNS).

For example, the CSF-1R inhibitor pexidartinib (PLX3397; Turalio) has been approved by the U.S. Food and Drug Administration for the treatment of tenosynovial giant cell tumors, an illness characterized by peripheral macrophage infiltration. PLX3397 displays a high affinity for CSF-1R (10 nM) and 2-fold selectivity over c-kit (20 nM)[13,14] and has been observed in cerebrospinal fluid, albeit at low concentrations, following oral administration, indicating brain penetrability in nonhuman primates.[15,16] A recent phase 1b trial in patients with mild cognitive impairment has been initiated with the CSF-1R inhibitor JNJ 40346527, and results from this are pending completion of the trial (https://clinicaltrials.gov/ct2/show/NCT04121208). An additional CSF-1R inhibitor, BLZ945, is in currently in a phase 2 trial in patients with amyotrophic lateral sclerosis (ALS) (https://clinicaltrials.gov/ct2/show/NCT04066244).

As a result, several efforts have been made to develop a high-affinity and brain-penetrant positron emission tomography (PET) radiotracer that binds preferentially to CSF-1R[14,17,18] in order to visualize microglial activation.[19−24] The most advanced radiotracer for the neuroimaging of CSF-1R is 5-cyano-*N*-(4-(4-[^{11}C]methylpiperazin-1-yl)-2-(piperidin-1-yl)-phenyl)furan-2-carboxamide ([^{11}C]CPPC).[2] Preclinical PET studies were carried out in mouse and nonhuman primate models of neuroinflammation showing the specific binding of [^{11}C]CPPC.[2] PET imaging in rodent models of CNS disease

Received: December 18, 2020
Accepted: February 23, 2021

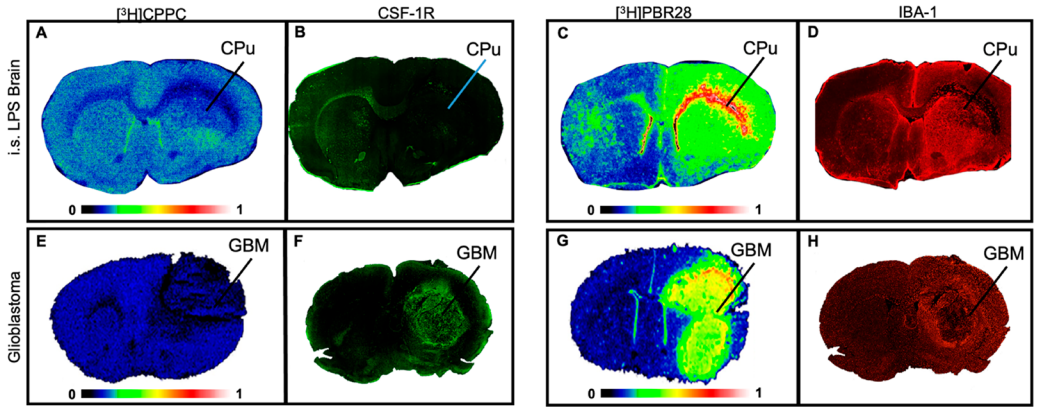

Figure 1. Distribution of inflammatory cells in LPS and GBM rodent models of neuroinflammation. [^{3}H]CPPC distribution in intrastriatal LPS rat and GBM mouse models does not align with inflammation as highlighted by [^{3}H]PBR28 autoradiography and IBA-1 immunofluorescence. (A) Representative autoradiography image of [^{3}H]CPPC (3 nM) binding density in the ipsilateral caudate putamen unilaterally injected with 4 μL of sterile saline containing 50 μg of LPS; Rats were sacrificed 7 days following injection. (B) Immunofluorescent staining with an anti-CSF-1R (green) antibody in the 7-day LPS injected rat brain tissue. (C) [^{3}H]PBR28 (3 nM) total binding to TSPO and (D) IBA-1 immunofluorescence (red) targeting microglia and macrogphages in the 7-day LPS injected rat brain tissue. (E) [^{3}H]CPPC (3 nM) total binding in a GBM mouse model. The unilateral injection of human GL251-Luc cells was carried out in mice. GBM sections display tumor burden 19 days after the injection of 2.5e^6 cells. (F) Anti-CSF-1R immunofluorescence (green) within the GBM mouse model brain tissues. (G) [^{3}H]PBR28 (3 nM) autoradiography in the GBM mouse model tissues. (H) IBA-1 immunofluorescence (red) in the GBM mouse model brain tissue. Intrastriatal (i.s.), caudate putamen (CPU; indicated by line, as assessed by anatomic brain atlas for rat); glioblastoma (GBM; indicated by line as assessed by anti-luciferase immunostaining (data not shown)).

have included transgenic AD mice and an experimental autoimmune encephalopathy (EAE) model of multiple sclerosis, which showed increased brain uptake in relevant brain regions of the disease. The radiopharmaceutical has recently been validated for human use, and preliminary human imaging has been performed.[25,26]

The present study aims to characterize [^{3}H]CPPC as an *in vitro* tool for applications in the CNS and periphery nervous system (PNS) and to screen a library of compounds derived from PLX3397 as potential PET imaging probes for CSF-1R. Specifically, preclinical *in vitro* studies were carried out using [^{3}H]CPPC to: (i) establish distribution of [^{3}H]CPPC in a rat intrastriatal lipopolysaccharide (LPS) and mouse glioblastoma (GL261-Luc; GBM) model of neuroinflammation compared to the 18 kDa translocator protein (TSPO) shown by [^{3}H]PBR28 autoradiography (ARG) and IBA-1 immunohistochemistry; (ii) determine the specific binding of [^{3}H]CPPC by ARG using CSF-1R targeting reference compounds in intrastriatal LPS rat brain tissues and intraperitoneal (ip) LPS mouse spleen tissues; (iii) compare the target density given by both [^{3}H]PBR28 and [^{3}H]CPPC binding in CNS tissues compared to peripheral tissues; (iv) explore selectivity over CNS targets and kinases and; (v) utilize [^{3}H]CPPC as a radioligand tool to screen novel therapeutics and diagnostic imaging agents in an array of compounds derived from PLX3397.

RESULTS AND DISCUSSION

Distribution of Inflammatory Cells in the CNS with Models of Neuroinflammation (LPS and glioblastoma). To establish the distribution of the binding of [^{3}H]CPPC in the CNS, robust rodent models of focal neuroinflammation were explored with LPS injection in addition to glioblastoma. The rodent models of LPS injection used adult male Sprague–Dawley rats sacrificed either 7-days or 30-days post-unilateral intrastriatal LPS injection (7-day LPS and 30-day LPS injection, respectively). ARG with [^{3}H]CPPC was performed to evaluate the distribution of CSF-1R specific binding in 7- (n = 2; Figure 1A) and 30-days (n = 3). [^{3}H]CPPC (3.5 nM) binding in 7-day post-LPS injection brain tissues showed little-to-no increase in the ipsilateral hemisphere (18.9 ± 1.7 nCi/mg; mean ± SD) compared to the contralateral hemisphere (17.9 ± 1.1 nCi/mg; mean ± SD, Figure 1A), as well as poor signal-to-noise ratio (49.9 ± 2.9% inhibition at 10 μM unlabeled CPPC). Representative CSF-1R immunostaining showed clustered target availability on the ipsilateral and contralateral hemispheres in 7-days intrastriatal LPS tissues. CSF-1R immunofluorescence was elevated in the contralateral corpus callosum (Figure 1B). Under conditions of central LPS-stimulated and GBM tumor-associated inflammation, microglia cells increase.[27] As such, a positive relationship with CSF-1R density is expected; however this was not observed *via* [^{3}H]CPPC ARG.

TSPO has been suggested to increase on microglia and macrophages when activated by neuroinflammatory processes. The second generation TSPO-targeting radioligand [^{3}H]PBR28 was used to establish the localization of inflammatory cells in LPS and glioblastoma CNS tissues. To support microglia distribution, IBA-1 immunofluorescence was employed. [^{3}H]PBR28 ARG showed robust and reproducible specific binding that was greatly elevated in the ipsilateral hemisphere of rats sacrificed 7-days post-surgery (83.5 ± 48.9 nCi/mg; mean ± SD) and 30-days post-surgery (36.2 ± 4.07 nCi/mg) compared to the contralateral hemisphere of each (29.0 ± 3.1 and 14.0 ± 2.36 nCi/mg, respectively; Figure 1C). TSPO distribution by [^{3}H]PBR28 aligned with IBA-1 immunostaining for microglia and macrophages in adjacent sections (Figure 1D) as the upregulation of TSPO occurs in these cell types under the conditions of neuroinflammation. Albeit, TSPO is also present on other cell types, as it is responsible for cholesterol transport within the outer membrane of the mitochondria.[24,28] Immunostaining using an anti-CSF-1R antibody showed localized regions of elevation within the ipsilateral and contralateral hemispheres of

https://dx.doi.org/10.1021/acschemneuro.0c00802
ACS Chem. Neurosci. XXXX, XXX, XXX−XXX

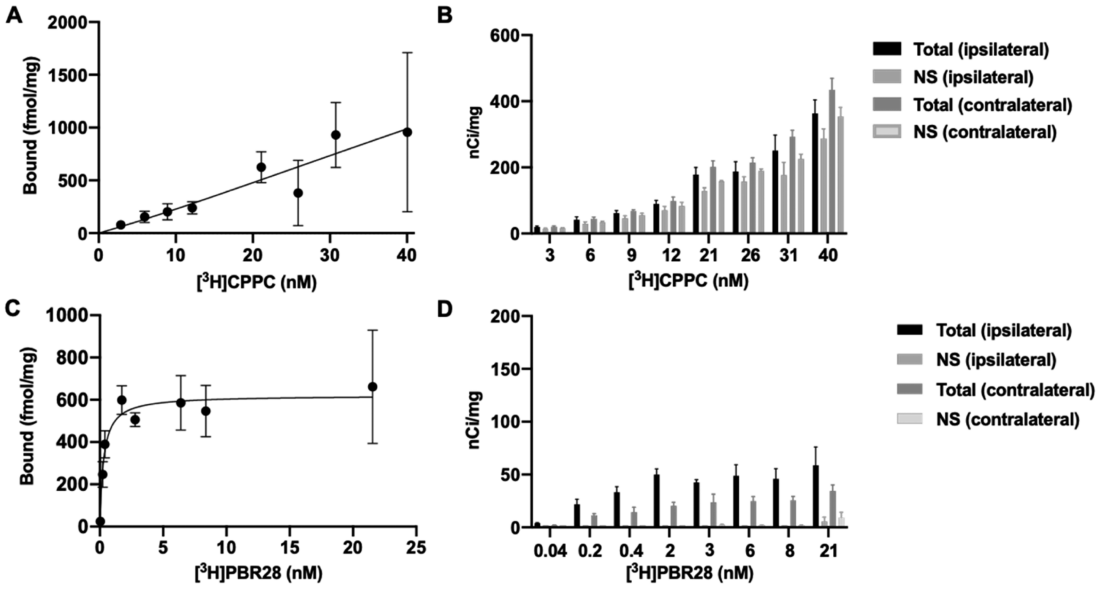

Figure 2. Saturability and distribution under conditions of increasing [^{3}H]CPPC (top) or [^{3}H]PBR28 (bottom) concentrations. [^{3}H]CPPC fails to saturate in the CNS tissues evaluated, where [^{3}H]PBR28 displays successful saturation. (A) Nonlinear regression fit of bound femtomole/milligram brain tissue using [^{3}H]CPPC performed by autoradiography analysis in 30-day post-injection intrastriatal LPS rat brain tissues (n = 3). (B) Total and nonspecific (10 μM CPPC) binding in the ipsilateral and contralateral hemispheres of injection in nanocurie/milligram tissue as determined by region of interest (ROI) analysis using tritium standards. (C) Nonlinear regression analysis of increasing [^{3}H]PBR28 concentrations in adjacent sections within the 30-day intrastriatal LPS brain tissues. (D) Increasing [^{3}H]PBR28 concentrations displaced by 10 μM FEPPA to define specific binding in the 7-day and 30-day LPS tissues.

injection; however, these regions did not align with [^{3}H]PBR28 and IBA-1 signals. This result may indicate a favorable specific labeling of a subset of the immune cell population by [^{3}H]CPPC in the LPS model, rather than an indication of overall immune cell expression.

Similar to the LPS model, brain tissues of a mouse model of human GBM also display an elevation of neuroinflammatory cells in the area of the tumor. Elevated CSF-1R has previously been reported in the immunostaining of human tissue arrays and a rodent GBM model.[29,30] In the present studies, a visualization of [^{3}H]CPPC (5 nM) binding was not present in the area of the tumor (Figure 1E) despite an elevation in CSF-1R immunostaining (Figure 1F). In contrast, a high [^{3}H]PBR28 specific signal was observed in the region of the tumor and immediately proximal areas (relative target density: 250 500 MDC/mm^2), corresponding to increased signals from IHC staining of markers for macrophages and microglia (Figure 1G). The distribution of [^{3}H]PBR28 aligned with IBA-1 immunostaining on adjacent tissue sections (Figure 1H). By comparison, the areas of decreased immunostaining for inflammatory cells exhibited a low [^{3}H]PBR28 binding density (620 MDC/mm^2). A lack of [^{3}H]CPPC signal in the tumor tissue at a 5 nM concentration suggests a lower affinity than that reported in the literature.[2,21] Concentrations of [^{3}H]CPPC employed in the present assay conditions (3.5 and 5 nM) were approximately 4.5- and 6-fold the reported half maximal inhibitory concentration (IC_{50}; 0.8 nM), respectively. The true binding affinity (K_d) of radiolabeled CPPC in mammalian tissues is yet to be reported *via* these methods, where K_d is the concentration at which one-half of the maximum number of binding sites is occupied. Though impacted by the concentration of radioligand used in the assay, the rationale for using the IC_{50} concentration serves as a valid approximation of the affinity while also providing adequate counts to elicit an *in vitro* binding signal. The lack of observed signal present and quantifiable at 5 nM [^{3}H]CPPC suggests that the true affinity in innate tissue is likely lower than the IC_{50} of 0.8 nM reported in noninnate protein target.[31] Further evidence is provided by the observation in mouse GBM brain sections that using an 18 nM concentration of [^{3}H]CPPC yields ~60% specific signal as defined using unlabeled 10 μM CPPC (Figure S1). Moreover, [^{3}H]CPPC binding density did not align with the observed distribution of inflammatory cells. PET imaging with [^{11}C]CPPC was able to show increased radioligand uptake and retention in a mouse model of LPS-induced inflammation 2 or 3 days after intracranial injection; however, the *ex vivo* evaluation of radioligand binding in these models did not corroborate the *in vivo* signal.[2] The inconsistent results between the *in vivo* and *in vitro* radioligand binding methods are unlikely to be attributed to physiochemical differences between labeling methods, for example, molar activity.

In contrast, [^{3}H]PBR28 (3 nM) ARG provided a measurable and increased signal in the area of the inflamed cells correlating to increased IBA-1 immunostaining on the ipsilateral hemisphere of LPS injection in both 7-day and 30-day post-LPS rat brain tissues and the GBM mouse model. CSF-1R expression has not been fully characterized within the time course of intrastriatal LPS injection, and the window of elevated receptor density may not align with the time points used in these studies. This model, under these time points, may not be optimized for the evaluation of [^{3}H]CPPC. However, strong anti-CSF-1R immunofluorescence was observed in the mouse GBM model in the absence of a [^{3}H]CPPC signal at an assay concentration above the reported IC_{50} for CSF-1R.[31] It should be noted that a lack of binding *in vitro* in the presence of robust immunostaining in the GBM tissues may also indicate a difference in receptor conformation post-mortem. Taken together, [^{3}H]CPPC distribution in intrastriatal LPS rat and the GBM mouse models does not

https://dx.doi.org/10.1021/acschemneuro.0c00802
ACS Chem. Neurosci. XXXX, XXX, XXX−XXX

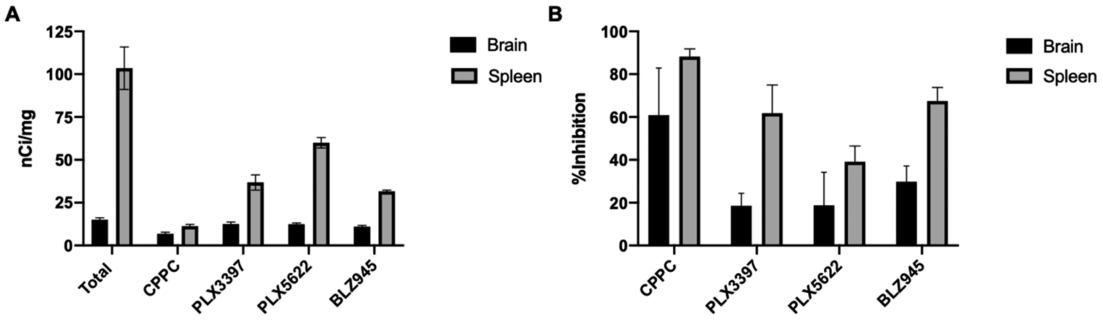

Figure 3. Specific binding of [^{3}H]CPPC in intrastriatal LPS rat brain tissue and ip LPS mouse spleen tissue. An increased [^{3}H]CPPC signal-to-noise ratio was observed in the ip LPS spleen tissue, compared to the intrastriatal LPS rat brain tissue . (A) Binding density (nanocurie/milligram tissue) of 3 nM [^{3}H]CPPC in 30-day LPS rat brain tissues (n = 3) and ip LPS mouse spleen tissue (n = 6) exposed to an equivalent volume of vehicle (DMSO) or 10 μM final concentration of unlabeled CPPC, PLX3397, PLX5622, or BLZ945. The bar graph displays mean ± SD. (B) Percent inhibition of 3 nM [^{3}H]CPPC is displayed as mean ± SD for 10 μM final concentration of unlabeled CPPC, PLX3397, PLX5622, or BLZ945. 100% binding was defined by 3 nM [^{3}H]CPPC with vehicle (DMSO).

align with inflammation as highlighted by [^{3}H]PBR28 autoradiography and IBA-1 immunofluorescence, suggesting that further assessment of [^{3}H]CPPC as a CSF-1R radioligand for CNS applications *via* saturation binding in neuroinflammatory models was warranted.

[^{3}H]CPPC Saturation Binding in Models of Neuroinflammation. To further explore the suitability of [^{3}H]CPPC as a CSF-1R radioligand tool, the quantitation of the target density (B_{max}) and K_d of [^{3}H]CPPC to CSF-1R were assessed using saturation binding methods. Under conditions of increasing [^{3}H]CPPC concentration, the specific binding window in the brain increased minimally and, in 30-day LPS treatment brain sections, failed to saturate up to a radioligand concentration of 40 nM (Figure 2A), using the rationale that this is approximately 40-fold above the reported binding affinity and thus an estimate of B_{max}. Furthermore, the [^{3}H]CPPC binding density did not increase on the ipsilateral side compared to the contralateral side of the injection site, and in some cases, the contralateral hemisphere displayed a higher binding than the side of injury (Figure 2B). This may be due to the presence of nonspecific binding of the radioligand, nondisplaceable off-target binding, or a lack of a sufficient target density in this model at this time point.

[^{3}H]PBR28 was utilized in this work as a control of the radioligand binding techniques employed to characterize CSF-1R targeting PET radioligands due to the favorable specific binding properties of [^{3}H]PBR28. To confirm saturability, increasing concentrations of [^{3}H]PBR28 quantified a B_{max} of 620.7 fmol/mg at the ipsilateral hemisphere of the 30-day LPS (Figure 2C). The total binding of [^{3}H]PBR28 was elevated on the ipsilateral side of injection compared to the contralateral side, and the nonspecific binding defined by 10 μM FEPPA, a TSPO-specific ligand,[32] displaced a greater than 95% of radioligand binding (Figure 2D). It is noteworthy that TSPO is present on cell types beyond microglia.[33] Nonetheless, [^{3}H]PBR28 displays a low nonspecific binding, which permits the quantification of B_{max} and K_d in this LPS model.

The poor specific binding observed *in vitro* in the rodent brain tissue with [^{3}H]CPPC prevents an accurate estimate of CSF-1R density in these post-mortem tissues by ARG. Although the LPS model of neuroinflammation has limitations (*vide supra*), [^{3}H]CPPC binding was observed in these tissues and was displaceable by 10 μM unlabeled CPPC up to 50% in the present conditions. Due to the nature of homologous competition, the displacement of specific and nonspecific sites of binding can result in the skewing of data toward a greater inhibition.

Specific Binding of [^{3}H]CPPC in the CNS and Periphery in Models of LPS-Induced Inflammation. Specific binding should be determined in the presence of a structurally dissimilar ligand (heterologous competition) to avoid the potential overestimation of true specific signal. Here, radioligand candidate binding to off-target and non-specific sites remain unidentified by competing with the unlabeled radioligand (homologous competition). In this case, the competition of [^{3}H]CPPC (3 nM) was carried out by comparing 10 μM CPPC to the same concentration of small molecule CSF-1R inhibitors PLX3397, PLX5622, and BLZ945. The quantitation of the ipsilateral hemisphere of 30-day LPS tissues shows 15 nCi/mg total binding (Figure 3A), while CPPC, PLX3397, PLX5622, and BLZ945 inhibited this binding by 60%, 15%, 16%, and 25%, respectively (Figure 3B). Heterologous binding was expected to produce a lower percentage of inhibition than homologous binding and is consistent with ARG studies performed with [^{11}C]CPPC.[2] Though a 60% specific binding window was observed with CPPC, a greater than 85% specific binding is preferable for the execution of concentration response curves to investigate novel compounds.

Due to the challenges of low CSF-1R density and high nonspecific binding in the LPS brain tissue, alternative tissues were explored to act as a positive control for CSF-1R expression. The spleen was identified as a tissue that possesses numerous peripheral macrophages expressing CSF-1R, and these tissues permitted both an increased baseline radioligand binding (100 nCi/mg, Figure 3A) and an improved signal-to-noise ratio. [^{3}H]CPPC (3 nM) was inhibited by CPPC, PLX3397, PLX5622, and BLZ945 by 85%, 60%, 40%, and 65%, respectively, in an ip LPS injection mouse model (n = 6; Figure 3B). [^{3}H]CPPC and [^{3}H]PBR28 were also evaluated for specific binding in the LPS-treated spleen and the 7-day and 30-day post-LPS injected brains under "No-Wash Assay" conditions described by Patel et al[34] (Figure S2). Under these conditions, there was a lack of specific binding with [^{3}H]CPPC in all tissues, compared to >60% specific binding of [^{3}H]PBR28 in the same tissues. The low specific binding of [^{3}H]CPPC under these *in vitro* conditions indicates that a poor specific signal would likely be observed *in vivo*, a factor that was highlighted by Jain et al.[20] Representative images demonstrate total [^{3}H]CPPC binding and adjacent tissues coincubated with

https://dx.doi.org/10.1021/acschemneuro.0c00802
ACS Chem. Neurosci. XXXX, XXX, XXX−XXX

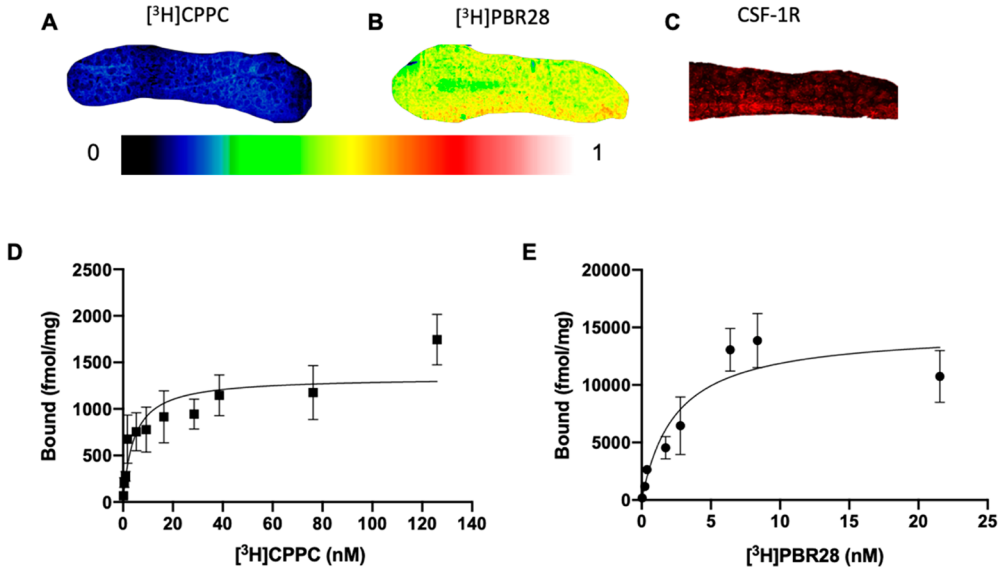

Figure 4. CSF-1R distribution and saturability in ip LPS spleen tissue. Both [^{3}H]CPPC and [^{3}H]PBR28 display successful saturation in ip LPS spleen tissue. Radioligand binding of (A) [^{3}H]CPPC (2 nM) and (B) [^{3}H]PBR28 (2 nM) in ip LPS mouse spleen tissue. (C) Immunofluorescent staining of CSF-1R in ip LPS mouse spleen tissue. Saturation analysis of (D) [^{3}H]CPPC and (E) [^{3}H]PBR28 in ip LPS spleen tissues.

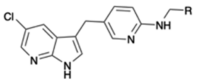

Cmpd	R	% Inhibited	Cmpd	R	% Inhibited	Cmpd	R	% Inhibited
1		77.5 ± 5.13	8		62.6 ± 4.5	15		50.4 ± 1.2
2		81.4 ± 0.27	9		52.0 ± 1.0	16		30.4 ± 0.7
3		37.1 ± 4.0	10		48.2 ± 2.7	17		50.8 ± 1.0
4		32.7 ± 6.1	11		54.3 ± 0.7	18		45.5 ± 1.3
5		78.9 ± 1.3	12		40.3 ± 1.2	19		48.5 ± 4.0
6		84.5 ± 0.5	13		70.8 ± 4.0	20		68.9 ± 0.9
7		61.0 ± 2.9	14		43.4 ± 5.7	21 (PLX3397)		61.8 ± 6.6

Figure 5. Percent inhibition of [^{3}H]CPPC by PLX3397 derivatives. Each value represents the mean ± SD of inhibition of each compound in a cross-section of whole ip LPS spleen from mice tissue (n = 6). Baseline binding with vehicle only (DMSO) was used to define 0% inhibition and 10 μM CPPC defined 100% inhibition.

CPPC, PLX3397, PLX5622, and BLZ945 in both intrastriatal LPS-treated brains and ip LPS-treated mouse spleens (Figure S3), with the improved displaceability by the CSF-1R inhibitors in the spleen compared to the brain tissues. The increased specific binding window in spleen tissues (>80% inhibition by 10 μM CPPC) is ideal for the evaluation of novel CSF-1R targeting compounds. Heterologous binding in spleen tissue displays decreased inhibition compared to homologous binding and is consistent with trends produced in LPS brain tissues. The percent inhibition in LPS brain tissue under these conditions is similar to that reported for [^{11}C]CPPC.[2] Using ARG, [^{11}C]CPPC binding was assessed in human post-mortem parietal lobe tissue from three AD cases and one control case. In total baseline conditions without the removal of nonspecific binding, a 75%−99% increase in [^{11}C]CPPC binding was reported. The evaluation of the specific binding of the [^{11}C]CPPC signal was carried out using CSF-1R inhibitors, unlabeled CPPC, compound **8**, BLZ945, and PLX3397. Inhibition by these compounds was reported as a ratio of total baseline binding to the inhibited condition. The greatest inhibition in AD tissues was observed by unlabeled CPPC (1.7−2.7), followed by compound **8** (2.0 ± 0.23), BLZ945 (1.79 ± 0.88), and PLX3397 (1.25 ± 0.25). Reference compounds targeting CSF-1R have been indicated to the present as type II or type I inhibitors binding an unphosphorylated inactive or autophosphosphorylated activation state, respectively.[35] This may contribute to the reduced and variable inhibition by the included reference compounds.

Comparison of [^{3}H]CPPC and [^{3}H]PBR28 in Spleen Tissues. The binding of [^{3}H]CPPC (Figure 4A) and

https://dx.doi.org/10.1021/acschemneuro.0c00802
ACS Chem. Neurosci. XXXX, XXX, XXX−XXX

[^{3}H]PBR28 (Figure 4B) at 2 nM radioligand concentration shows displaceable binding in ip LPS spleen tissues. The immunofluorescent staining of CSF-1R in the spleen shows target availability. The observed binding density of [^{3}H]PBR28 is elevated compared to that of [^{3}H]CPPC, and saturation analysis was performed to quantify these differences. Unlike brain tissues, [^{3}H]CPPC saturated in spleen tissue from the ip LPS mouse model of inflammation. Under the conditions of increasing [^{3}H]CPPC concentration, radioligand binding plateaus and calculates a B_{max} of 1339 fmol/mg tissue and a K_d of 4.3 nM (Figure 4D). Adjacent sections of the spleen treated with an increasing concentration of [^{3}H]PBR28 show saturability and quantified a B_{max} of 14771 fmol/mg tissue and a K_d of 2.4 nM (Figure 4E), and a specific binding of 99 ± 0.03% was defined using 10 μM of unlabeled FEPPA to carry-out heterologous binding.[32] This target density is more than 10-fold higher for TSPO in spleen tissue than CSF-1R; however, TSPO is noted in the literature to be expressed on a greater number of cell types.[33]

***In Vitro* Screening of CSF-1R Targeting Compounds in Spleen Tissue Using [^{3}H]CPPC.** To demonstrate the potential application of [^{3}H]CPPC in drug development for neuroinflammation pharmacology, we evaluated an array of 20 derivatives of PLX3397 in spleen tissue, with the goal of identifying a novel high-affinity CSF-1R selective compound as a next-generation PET radiotracer. By employing the most promising assay conditions observed, the structural derivatives of PLX3397 (Figure 5) were investigated by ARG in the ip LPS mouse spleen tissue. A concentration of radioligand yielding the highest signal-to-noise ratio was chosen following saturation analysis. A minimal criterion of 80% inhibition was required for a compound to pass the initial screen. Of the 20 PLX3397 derivatives, two compounds (**2** and **6**) exceeded this initial criterion at a concentration of 6.6 nM [^{3}H]CPPC displaced by a 10 μM concentration of each compound. Additionally, compound **1** was minimally below the cutoff criteria (77.5% inhibition) and was included with compounds **2** and **6** for further screening due to the structural ease for tritiomethylation (Figure 5).

To rank-order the compounds by apparent affinity (K_i), concentration response curves (Figure 6A) were generated for each compound yielding IC_{50} values that were converted to apparent affinity (Figure 6B) using the Cheng–Prussof equation.[36] Although the identified leads displayed micromolar K_i values (>1 μM) for CSF-1R when using [^{3}H]CPPC as a screening tool, compound **1** was chosen for further evaluation due to the aforementioned structural ease for tritiomethylation. The assay conditions employed resulted in minimal specific binding in rodent CNS tissues and was determined to be not useful for further development (Figures S4 and S5).

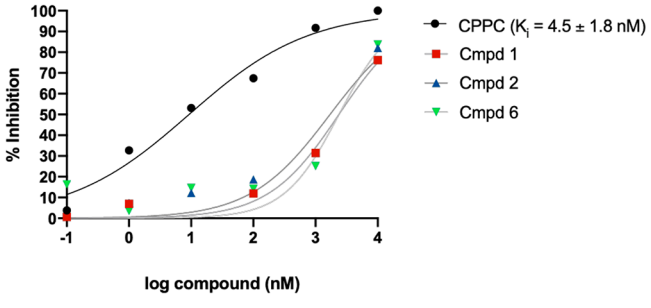

Figure 6. Concentration response curves of PLX3397 derivatives. Nonlinear regression analysis plots percent inhibition of [^{3}H]CPPC binding by increasing concentrations of unlabeled PLX-3397 derivatives **1**, **2**, and **6** curves. CPPC (10 μM) was used to normalize NS as 100% inhibition and baseline nanocurie/milligram was used to define 0% inhibition. The Cheng–Prusoff equation was used to convert IC_{50} to K_i. NS, nonspecific binding. PLX3397 derivatives (compounds **1**, **2**, and **6**) had K_i > 1 μM.

The determined IC_{50} (9.4 nM) was converted to K_i using the K_d established by saturation binding experiments in ip LPS spleen tissue. The K_i (4.5 nM) is approximately 5.6-fold higher than the reported IC_{50} for CPPC.[31] The compounds identified from the PLX3397-derivative library yielded K_i values in the micromolar range, far above the low to subnanomolar affinity required for successful PET imaging agents. The hill slope (nH) may be used as an indicator of the number of binding populations, with shallow curves sometimes indicating more than one compound–target interaction. Under these conditions, the CPPC concentration curve resulted in a hill slope of 0.46, consistent with multiple binding sites with different affinities for CPPC.

Illig et al. noted off-target binding of CPPC (compound **8**) to kinases Kit, Axl, TrkA, Flt-3, and IRKβ at concentrations less than 0.1 μM.[31] In light of this potential selectivity concern with CPPC, a scanMAX KINOMEscan profile of 403 known kinases (Table S1) and a CNS safety panel of 78 known targets (Table S2) were solicited (Eurofins DiscoverX Corporation, San Diego, CA). The kinase panels identified a number of off-target kinases at a concentration (10 μM) of unlabeled CPPC relevant to *in vitro* radioligand binding assays. The Eurofins DiscoverX SAFETYscan identified three CNS targets with IC_{50} values in the micromolar range including the serotonin 5-HT3A receptor (5.86 μM), $\alpha4\beta2$ nicotinic acetylcholine receptor (4.88 μM), and the NAV 1.5 sodium-gated channel (6.51 μM). Expectedly, three kinase hits yielded submicomolar IC_{50} values including an insulin receptor (0.070 μM), tyrosine protein kinase LCK (0.022 μM), and vascular endothelial growth factor receptor 2 (0.074 μM). On the basis of the IC_{50} values generated from the CNS safety panel for the three kinase hits, [^{3}H]CPPC used at saturating concentrations would likely confound the analysis of the interaction of [^{3}H]CPPC with CSF-1R. Without the affinity values of CPPC to the numerous hits identified by the kinase screen, conclusions pertaining to the selectivity of [^{11}C]CPPC cannot be made from this study. For use as an *in vitro* radioligand tool for screening putative CSF-1R targeting compounds, where a balance of the signal-to-noise ratio and using a concentration high enough for detection by the methods employed in these studies, [^{3}H]CPPC was useful in the absence of an alternative ^{3}H-labeled CSF-1R inhibitor but comes with caveats of potential off-target binding sites. Structure–activity relationships based on CPPC or PLX-3397 should consider off-target binding for PET radiotracer design.

CONCLUSIONS

Herein, we report the first *in vitro* evaluation of [^{3}H]CPPC as a radioligand tool in several rodent models of neuroinflammation where both adequate saturability or specific binding were not observed. The nonspecific binding of [^{3}H]CPPC was high in normal rodent brain tissue. When compared to TSPO ([^{3}H]PBR28) binding and IBA-1 immunofluorescence, [^{3}H]CPPC did not align with the expression of inflammation and appeared to have a lower affinity than previously reported. Because of the poor signal-to-noise ratio observed in CNS

https://dx.doi.org/10.1021/acschemneuro.0c00802
ACS Chem. Neurosci. XXXX, XXX, XXX–XXX

tissues, saturation binding assays were carried out in LPS-treated spleen tissues. A B_{max} of 1339 fmol/mg and a K_d for CSF-1R of 4.3 nM were calculated with [^{3}H]CPPC. Using this *in vitro* assay system, [^{3}H]CPPC was applied to screen a novel library of CSF-1R inhibitors as potential PET radioligand leads, where the potential for multiple binding sites was observed. The target selectivity of CPPC was then evaluated against 403 kinases and 78 CNS targets, where it was found to inhibit several CNS targets and kinases. Due to the identified off-target binding and low specific binding in the CNS under the employed conditions, [^{3}H]CPPC may not be a suitable radioligand tool for the *in vitro* evaluation of novel CSF-1R targeting compounds.

MATERIALS AND METHODS

General. Radiolabeled [^{3}H]5-cyano-*N*-(4-(4-methylpiperazin-1-yl)-2-(piperidin-1-yl)phenyl)furan-2-carboxamide ([^{3}H]CPPC) (80 Ci/mmol; 1 mCi/mL) was prepared by Novandi Chemistry AB (Södertälje, Sweden) along with the reference compound CPPC. When stored at −20 °C in ethanol, the rate of decomposition of [^{3}H]CPPC is less than 3% over the first 6 months, with measurements taken at 2, 4, and 6 months. The experiments were all carried out within the first two months following radiosynthesis. CSF-1R inhibitor and parent compound, 5-((5-chloro-1*H*-pyrrolo[2,3-*b*]-pyridin-3-yl)methyl)-*N*-((6-(trifluoromethyl)pyridin-3-yl)methyl)-pyridin-2-amine (PLX3397, **21**), and tyrosine kinase inhibitor GW2580 were purchased from Cedarlane (Burlington, ON, Canada). LPS was purchased from Sigma-Aldrich (St. Louis, MO). For the evaluation of fresh-frozen intrastriatal LPS rat brain tissues, an anti-IBA-1(635)-conjugated antibody was obtained from FUJIFILM Wako. An anti-CSF-1R (SP211) primary antibody was purchased from Abcam (Cambridge, MA) and was used in intrastriatal LPS rat brain and ip LPS mouse spleen tissues as well as GBM mouse brain tissues.

Compound Synthesis. Potential CSF-1R ligands are shown in Figure 5. Compound structures were derived from the structure **21** and supplied by MedChem Imaging, Inc. (Boston, MA).

Neuroinflammation Models. Rodent models of neuroinflammation were generated in-house under the approval of the institutional animal care and use committee. A rat model of acute neuroinflammation was generated by the unilateral intrastriatal injection of LPS. Adult male Sprague−Dawley rats (n = 5; 250−300 g) were anesthetized and positioned in a stereotactic head frame. Neuroinflammation was induced by a single striatal injection of 50 μg of LPS dissolved in 4 μL of sterile saline at a flow rate of 0.5 μL/min. Rats were sacrificed at 7- or 30-days post-injection.

A model of subchronic neuroinflammation was generated as previously described by Neal et al.[11] Adult male C57bl/6 mice (10 weeks) were intraperitoneally (ip) administered 1 mg/kg LPS dissolved in normal saline for 3 (n = 6) or 4 (n = 4) consecutive days and sacrificed on day 5 or 6, respectively.

Glioblastoma Model. A mouse model of glioblastoma was generated by InviCRO, LLC (San Diego, CA). Cells at a concentration of 2.5e^6 were injected unilaterally into the striatum. Ten days later, an MRI was performed to select mice with tumor burden for enrollment into the study. Mice were euthanized 9 days later on the basis of determined MRI tumor volumes and processed for formalin-fixed paraffin-embedded (FFPE) immunohistochemistry. Tissues for ARG were fresh-frozen for analysis.

Tissue Section Preparation. For ARG and immunostaining, rodents were sacrificed and brains and spleens were slow-frozen in powdered dry ice. Fresh-frozen brains were cryosectioned (Leica CM3050S; 10 μm), thaw-mounted on glass slides, and stored at −80 °C for later use.

Autoradiography. CSF-1R ARG was carried out with modifications in accordance with Horti et al.[2] To evaluate specific binding, tissues were incubated with 3 or 6 nM [^{3}H]CPPC with a 10 μM reference compound (unlabeled CPPC, PLX3397, PLX5622, BLZ945, GW2580, 6-OH BTA) or a vehicle in 100% fetal bovine serum for 2 h at room temperature. Tissue sections were subsequently washed with 0.5% bovine serum albumin (4 °C) and deionized water (4 °C). Slides were air-dried and exposed to phosphorscreens (BAS-IP TR4020; GE Healthcare) for 5 days. Images were generated by scanning with an Amersham Typhoon phosphorimager (GE Healthcare). Region of interest (ROI) analysis was performed using MCID 7.0 imaging suite (Interfocus Imaging, Cambridge, UK). Raw nanocurie/milligram, percent specific binding, or percent inhibition are reported. For saturation analysis, tissue sections were incubated with ascending concentrations of the radioligand under the same conditions described. Nonspecific binding was defined by 10 μM CPPC, alone.

Immunofluorescence. Fresh-frozen intrastriatal LPS rat tissues were acclimated to room temperature and then exposed to post-fixation by acetone. Formalin-fixed paraffin embedded GBM brain tissue sections were deparaffinized and underwent antigen retrieval by sodium citrate (pH 6) for 20 min. Following a 10 min wash in wash buffer (tris-HCl buffered saline (TBS) containing 0.1% Triton-X), tissues were exposed to animal-free protein block (Vector laboratories; Burlingame, CA). Tissues were incubated with rabbit anti-IBA-1(635)-conjugated primary antibody (Fujifilm Wako), anti-CSF-1R (SP211; Abcam, Cambridge, MA), or antibody diluent overnight at 4 °C and then washed with TBS buffer 3 × 5 min. For CSF-1R detection, a goat anti-rabbit secondary antibody conjugated to Alexa-Fluor-488 was applied at room temperature for 60 min. Following washing and 10 min incubation with DAPI, slides were washed with distilled water and coverslipped. Slides were imaged using a Zeiss Axioscan Z.1 (Zeiss) and an Olympus VS200 (Olympus Corporation).

ASSOCIATED CONTENT

Supporting Information

The Supporting Information is available free of charge at https://pubs.acs.org/doi/10.1021/acschemneuro.0c00802.

Figures of representative image of specific binding in GBM model at a concentration higher than K_d, no wash assay results, representative autoradiography images, ROI analysis, and percent inhibition of 6 nM [^{3}H]CPPC, tables of results of KINOMEscan scanMAX profile, results of Eurofins DiscoverX SAFETY scan, and CNS MPO calculation for CPPC, and discussions of compounds, radioligands, and reagents used, cell preparation, autoradiography, no wash assay, cell filtration binding assays, and immunohistochemistry (PDF)

AUTHOR INFORMATION

Corresponding Authors

Shil Patel − *Codiak Biosciences, Cambridge, Massachusetts 02140, United States*; Phone: +1 857 949 4139; Email: Shil.Patel@codiakbio.com

Neil Vasdev − *Azrieli Centre for Neuro-Radiochemistry, Brain Health Imaging Centre, Centre for Addiction and Mental Health (CAMH), Toronto, ON M5T 1R8, Canada; Institute of Medical Science, University of Toronto, Toronto, ON M5S 1A8, Canada; Division of Nuclear Medicine and Molecular Imaging, Massachusetts General Hospital and Department of Radiology, Harvard Medical School, Boston, Massachusetts 02114, United States; MedChem Imaging, Inc., Boston, Massachusetts 02210, United States;* orcid.org/0000-0002-2087-5125; Phone: +1 416 535 8501 ext 30988; Email: Neil.Vasdev@utoronto.ca

https://dx.doi.org/10.1021/acschemneuro.0c00802
ACS Chem. Neurosci. XXXX, XXX, XXX−XXX

Authors

Ashley C. Knight − *Azrieli Centre for Neuro-Radiochemistry, Brain Health Imaging Centre, Centre for Addiction and Mental Health (CAMH), Toronto, ON M5T 1R8, Canada; Institute of Medical Science, University of Toronto, Toronto, ON M5S 1A8, Canada;* orcid.org/0000-0003-2225-360X

Cassis Varlow − *Azrieli Centre for Neuro-Radiochemistry, Brain Health Imaging Centre, Centre for Addiction and Mental Health (CAMH), Toronto, ON M5T 1R8, Canada; Institute of Medical Science, University of Toronto, Toronto, ON M5S 1A8, Canada*

Tong Zi − *Codiak Biosciences, Cambridge, Massachusetts 02140, United States*

Steven H. Liang − *Division of Nuclear Medicine and Molecular Imaging, Massachusetts General Hospital and Department of Radiology, Harvard Medical School, Boston, Massachusetts 02114, United States;* orcid.org/0000-0003-1413-6315

Lee Josephson − *Division of Nuclear Medicine and Molecular Imaging, Massachusetts General Hospital and Department of Radiology, Harvard Medical School, Boston, Massachusetts 02114, United States; MedChem Imaging, Inc., Boston, Massachusetts 02210, United States*

Karl Schmidt − *Codiak Biosciences, Cambridge, Massachusetts 02140, United States*

Complete contact information is available at: https://pubs.acs.org/10.1021/acschemneuro.0c00802

Author Contributions

A.C.K., C.V., T.Z., S.P. N.V., L.J., S.H.L., and K.S. designed the research. A.C.K., T.Z., C.V., S.P., and S.H.L. performed the research. A.C.K., C.V., T.Z., S.P., S.H.L., N.V., L.J., and K.S. contributed new reagents/analytical tools and analyzed data. A.C.K., C.V., S.P., and N.V. wrote the paper. A.C.K., S.P., and N.V. oversaw the project.

Notes

The authors declare the following competing financial interest(s): L.J. and N.V. are co-founders and S.H.L is a consultant of MedChem Imaging, Inc. All other authors declare no conflict of interest.

■ ACKNOWLEDGMENTS

N.V. would like to thank the National Institute on Ageing of the NIH (R01AG054473 and R01AG052414), the Azrieli Foundation, Canada Foundation for Innovation, Ontario Research Fund, and the Canada Research Chairs Program. We greatly appreciate the support of Dr. Richard Hargreaves, as well as members of the CAMH Brain Health Imaging Centre.

■ REFERENCES

(1) Obst, J., Simon, E., Mancuso, R., and Gomez-Nicola, D. (2017) The Role of Microglia in Prion Diseases: A Paradigm of Functional Diversity. *Front. Aging Neurosci. 9*, 207.

(2) Horti, A. G., Naik, R., Foss, C. A., Minn, I., Misheneva, V., Du, Y., Wang, Y., Mathews, W. B., Wu, Y., Hall, A., et al. (2019) PET imaging of microglia by targeting macrophage colony-stimulating factor 1 receptor (CSF1R). *Proc. Natl. Acad. Sci. U. S. A. 116*, 1686−1691.

(3) Stanley, E. R., and Chitu, V. (2014) CSF-1 receptor signaling in myeloid cells. *Cold Spring Harbor Perspect. Biol. 6*, a021857.

(4) Elmore, M. R., Najafi, A. R., Koike, M. A., Dagher, N. N., Spangenberg, E. E., Rice, R. A., Kitazawa, M., Matusow, B., Nguyen, H., West, B. L., et al. (2014) Colony-stimulating factor 1 receptor signaling is necessary for microglia viability, unmasking a microglia progenitor cell in the adult brain. *Neuron 82*, 380−397.

(5) Tang, R., Beuvon, F., Ojeda, M., Mosseri, V., Pouillart, P., and Scholl, S. (1992) M-CSF (monocyte colony stimulating factor) and M-CSF receptor expression by breast tumour cells: M-CSF mediated recruitment of tumour infiltrating monocytes? *J. Cell. Biochem. 50*, 350−356.

(6) Akiyama, H., Nishimura, T., Kondo, H., Ikeda, K., Hayashi, Y., and McGeer, P. L. (1994) Expression of the receptor for macrophage colony stimulating factor by brain microglia and its upregulation in brains of patients with Alzheimer's disease and amyotrophic lateral sclerosis. *Brain Res. 639*, 171−174.

(7) Akiyama, H., Barger, S., Barnum, S., Bradt, B., Bauer, J., Cole, G. M., Cooper, N. R., Eikelenboom, P., Emmerling, M., Fiebich, B. L., et al. (2000) Inflammation and Alzheimer's disease. *Neurobiol. Aging 21*, 383−421.

(8) Spangenberg, E., Severson, P. L., Hohsfield, L. A., Crapser, J., Zhang, J., Burton, E. A., Zhang, Y., Spevak, W., Lin, J., and Phan, N. Y. (2019) Sustained microglial depletion with CSF1R inhibitor impairs parenchymal plaque development in an Alzheimer's disease model. *Nat. Commun. 10*, 3758.

(9) Sosna, J., Philipp, S., Albay, R., Reyes-Ruiz, J. M., Baglietto-Vargas, D., LaFerla, F. M., and Glabe, C. G. (2018) Early long-term administration of the CSF1R inhibitor PLX3397 ablates microglia and reduces accumulation of intraneuronal amyloid, neuritic plaque deposition and pre-fibrillar oligomers in 5XFAD mouse model of Alzheimer's disease. *Mol. Neurodegener. 13*, 11.

(10) Olmos-Alonso, A., Schetters, S. T., Sri, S., Askew, K., Mancuso, R., Vargas-Caballero, M., Holscher, C., Perry, V. H., and Gomez-Nicola, D. (2016) Pharmacological targeting of CSF1R inhibits microglial proliferation and prevents the progression of Alzheimer's-like pathology. *Brain 139*, 891−907.

(11) Neal, M. L., Fleming, S. M., Budge, K. M., Boyle, A. M., Kim, C., Alam, G., Beier, E. E., Wu, L.-J., and Richardson, J. R. (2020) Pharmacological inhibition of CSF1R by GW2580 reduces microglial proliferation and is protective against neuroinflammation and dopaminergic neurodegeneration. *FASEB J. 34*, 1679−1694.

(12) Mancuso, R., Fryatt, G., Cleal, M., Obst, J., Pipi, E., Monzón-Sandoval, J., Ribe, E., Winchester, L., Webber, C., Nevado, A., et al. (2019) CSF1R inhibitor JNJ-40346527 attenuates microglial proliferation and neurodegeneration in P301S mice. *Brain 142*, 3243−3264.

(13) Cannarile, M. A., Weisser, M., Jacob, W., Jegg, A. M., Ries, C. H., and Rüttinger, D. (2017) Colony-stimulating factor 1 receptor (CSF1R) inhibitors in cancer therapy. *J. Immunother. Cancer 5*, 53.

(14) Tanzey, S. S., Shao, X., Stauff, J., Arteaga, J., Sherman, P., Scott, P. J. H., and Mossine, A. V. (2018) Synthesis and Initial In Vivo Evaluation of [^{11}C]AZ683-A Novel PET Radiotracer for Colony Stimulating Factor 1 Receptor (CSF1R). *Pharmaceuticals 11*, 136.

(15) Shankarappa, P. S., Peer, C. J., Odabas, A., McCully, C. L., Garcia, R. C., Figg, W. D., and Warren, K. E. (2020) Cerebrospinal fluid penetration of the colony-stimulating factor-1 receptor (CSF-1R) inhibitor, pexidartinib. *Cancer Chemother. Pharmacol. 85*, 1003−1007.

(16) Odabas, A., McCully, C. M. L., Cruz, R., Figg, W. D., Glod, J., Rymar, A., Peer, C., and Warren, K. E. (2018) Phrm-03. Cerebrospinal fluid penetration of pexidartinib (PLX3397), A CSF1R inhibitor, in a nonhuman primate model. *Neuro. Oncol. 20*, i157.

(17) Naik, R., Misheneva, V., Minn, I., Melnikova, T., Mathews, W., Dannals, R., Pomper, M., Savonenko, A., Pletnikov, M., and Horti, A. (2018) PET tracer for imaging the macrophage colony stimulating factor receptor (CSF1R) in rodent brain. *J. Nucl. Med. 59*, 547.

(18) Bernard-Gauthier, V., and Schirrmacher, R. (2014) 5-(4-((4-[^{18}F]Fluorobenzyl)oxy)-3-methoxybenzyl)pyrimidine-2,4-diamine: a

selective dual inhibitor for potential PET imaging of Trk/CSF-1R. *Bioorg. Med. Chem. Lett. 24*, 4784−4790.
(19) Narayanaswami, V., Dahl, K., Bernard-Gauthier, V., Josephson, L., Cumming, P., and Vasdev, N. (2018) Emerging PET Radiotracers and Targets for Imaging of Neuroinflammation in Neurodegenerative Diseases: Outlook Beyond TSPO. *Mol. Imaging 17*, 153601211879231.
(20) Jain, P., Chaney, A. M., Carlson, M. L., Jackson, I. M., Rao, A., and James, M. L. (2020) Neuroinflammation PET Imaging: Current Opinion and Future Directions. *J. Nucl. Med. 61*, 1107−1112.
(21) Janssen, B, and Mach, R. H. (2019) Development of brain PET imaging agents: Strategies for imaging neuroinflammation in Alzheimer's disease. Progress in Molecular Biology and Translational Science in *Brain Imaging* (Becker, J. T., and Cohen, A. D.) 1st Ed., pp 371−399, Academic Press.
(22) Janssen, B., Vugts, D. J., Windhorst, A. D., and Mach, R. H. (2018) PET Imaging of Microglial Activation-Beyond Targeting TSPO. *Molecules 23*, 607.
(23) Downer, O. M., Marcus, R. E. G., Zürcher, N. R., and Hooker, J. M. (2020) Tracing the History of the Human Translocator Protein to Recent Neurodegenerative and Psychiatric Imaging. *ACS Chem. Neurosci. 11*, 2192−2200.
(24) Zhang, L., Hu, K., Shao, T., Hou, L., Zhang, S., Ye, W., Josephson, L., Meyer, J. H., Zhang, M.-R., Vasdev, N., et al. (2021) Recent developments on PET radiotracers for TSPO and their applications in neuroimaging. *Acta Pharm. Sin. B 11*, 373−393.
(25) Pomper, M. (2020) Imaging brain inflammatory states: Focus on CSF-1R, virtual, October 5−6, Alzheimer's Drug Discovery Foundation.
(26) Mathews, W. B., Wu, Y., Horti, A. G., Naik, R., Hall, A. W., Holt, D. P., and Dannals, R. F. (2019) Radiosynthesis and validation of [5-cyano-N-(4-(4-[^{11}C]methylpiperazin-1-yl)-2-(piperidin-1-yl)-phenyl) furan-2-carboxamide] ([^{11}C]CPPC), a PET radiotracer for imaging CSF1R, a microglia-specific marker. *J. Labelled Compd. Radiopharm. 62*, 903−908.
(27) Komohara, Y., Ohnishi, K., Kuratsu, J., and Takeya, M. (2008) Possible involvement of the M2 anti-inflammatory macrophage phenotype in growth of human gliomas. *J. Pathol. 216*, 15−24.
(28) Cumming, P., Burgher, B., Patkar, O., Breakspear, M., Vasdev, N., Thomas, P., Liu, G. J., and Banati, R. (2018) Sifting through the surfeit of neuroinflammation tracers. *J. Cereb. Blood Flow Metab. 38*, 204−224.
(29) Sun, L., Liang, H., Yu, W., and Jin, X. (2019) Increased invasive phenotype of CSF-1R expression in glioma cells via the ERK1/2 signaling pathway. *Cancer Gene Ther. 26*, 136−144.
(30) Cho, H. R., Jeon, H., Park, C. K., Park, S. H., and Choi, S. H. (2018) Radiogenomics Profiling for Glioblastoma-related Immune Cells Reveals CD49d Expression Correlation with MRI parameters and Prognosis. *Sci. Rep. 8*, 16022.
(31) Illig, C. R., Chen, J., Wall, M. J., Wilson, K. J., Ballentine, S. K., Rudolph, M. J., DesJarlais, R. L., Chen, Y., Schubert, C., Petrounia, I., et al. (2008) Discovery of novel FMS kinase inhibitors as anti-inflammatory agents. *Bioorg. Med. Chem. Lett. 18*, 1642−1648.
(32) Wilson, A. A., Garcia, A., Parkes, J., McCormick, P., Stephenson, K. A., Houle, S., and Vasdev, N. (2008) Radiosynthesis and initial evaluation of [^{18}F]-FEPPA for PET imaging of peripheral benzodiazepine receptors. *Nucl. Med. Biol. 35*, 305−314.
(33) Gui, Y., Marks, J. D., Das, S., Hyman, B. T., and Serrano-Pozo, A. (2020) Characterization of the 18 kDa translocator protein (TSPO) expression in post-mortem normal and Alzheimer's disease brains. *Brain Pathol. 30*, 151−164.
(34) Patel, S., Hamill, T., Hostetler, E., Burns, H. D., and Gibson, R. E. (2003) An in vitro assay for predicting successful imaging radiotracers. *Mol. Imaging Biol., 5*, 65−71.
(35) Wodicka, L. M., Ciceri, P., Davis, M. I., Hunt, J. P., Floyd, M., Salerno, S., Hua, X. H., Ford, J. M., Armstrong, R. C., Zarrinkar, P. P., and Treiber, D. K. (2010) Activation State-Dependent Binding of Small Molecule Kinase Inhibitors: Structural Insights from Biochemistry. *Chem. Biol. 17*, 1241−1249.
(36) Cheng, Y., and Prusoff, W. H. (1973) Relationship between the inhibition constant (K1) and the concentration of inhibitor which causes 50% inhibition (IC_{50}) of an enzymatic reaction. *Biochem. Pharmacol. 22*, 3099−3108.

https://dx.doi.org/10.1021/acschemneuro.0c00802
ACS Chem. Neurosci. XXXX, XXX, XXX−XXX